

RSC Advances



This is an *Accepted Manuscript*, which has been through the Royal Society of Chemistry peer review process and has been accepted for publication.

Accepted Manuscripts are published online shortly after acceptance, before technical editing, formatting and proof reading. Using this free service, authors can make their results available to the community, in citable form, before we publish the edited article. This *Accepted Manuscript* will be replaced by the edited, formatted and paginated article as soon as this is available.

You can find more information about *Accepted Manuscripts* in the [Information for Authors](#).

Please note that technical editing may introduce minor changes to the text and/or graphics, which may alter content. The journal's standard [Terms & Conditions](#) and the [Ethical guidelines](#) still apply. In no event shall the Royal Society of Chemistry be held responsible for any errors or omissions in this *Accepted Manuscript* or any consequences arising from the use of any information it contains.



Journal Name

COMMUNICATION

Porous N-Doped Graphitic Carbons Assembled One-Dimensional Hollow Structures as High Performance Electrocatalyst for ORR

Qiong Luo,^a Liyong Chen,^{*a} Binhua Duan,^a Zhizhi Gu,^a Jing Liu,^a Meiling Xu,^a Chunying Duan^{*a}

Received 00th January 20xx,
Accepted 00th January 20xx

DOI: 10.1039/x0xx00000x

www.rsc.org/

Nitrogen (N)-doped graphitic carbons with one-dimensional hollow/porous structures were synthesized via a sacrificial template of CdTe@ZIF-8 nanofibers. The N-doped graphitic carbons exhibited better electrocatalytic activity for ORR based on higher diffusion-limited current density and more positive half-wave potential as compared to carbons derived from ZIF-8.

Oxygen reduction reaction (ORR) is a critical process for electrochemical energy storage and conversion devices such as fuel cell and metal-air batteries.¹⁻³ However, the sluggish ORR kinetics at the cathode is the key issue to hinder the development of these energy-related devices.⁴ Albeit platinum (Pt)-based catalysts are the most efficient towards ORR, the scarce resource and poor durability caused by aggregation and leaching of Pt confine their large-scale practical use in these devices.^{5, 6} Therefore, utilization of non-precious metals or metal-free materials as ORR catalysts is needed to build electrochemical energy-related devices with high performance.^{7, 8} Among such classes of catalysts, heteroatom-doped graphitic carbons represent a typical candidate for metal-free catalysts towards ORR based on their tunable electronic properties and stable chemical properties, as well as abundant available carbon resources.⁹

Apart from the intrinsic component determining the charge distribution and electronic properties of graphitic carbons,¹⁰⁻¹⁴ the microstructures of graphitic carbons also played a decisive role in affecting mass transport and electron-transfer resistance during catalytic process.^{15, 16} The purpose of this paper is to explore electrocatalytic performance of one-dimensional porous and hollow N-doped graphitic carbons (denoted as One-H/P-C) towards ORR. One-H/P-C was synthesized by a sacrificial template route of anisotropic shaped metal-organic frameworks (MOFs). Based on the plain

synthetic system and the high content of N in ligands, zeolitic imidazolate framework-8 ($\text{Zn}(\text{mim})_2$ (ZIF-8); Hmim = 2-methylimidazole; mim = deprotonated 2-methylimidazole) was employed as an effective precursor for synthesis of One-H/P-C via pyrolysis (Fig. S1).^{12, 16-19} ZIF-8 with sodalite topology possesses a cubic space group $\bar{1}4\bar{3}$, thus, it is difficult to achieve the anisotropic morphologies by merely regulating the parameters of reaction system to overcome its isotropic feature of intrinsic crystalline structures.^{20, 21} According to an affinity between ZIF-8 and polyvinylpyrrolidone (PVP) molecules, PVP modified CdTe nanowires (PVP-CdTe NWs) can be served as templates inducing ZIF-8 heterogeneous nucleation and growth to form CdTe@ZIF-8 nanofibers. The nanofibers can be further applied to preparation of One-H/P-C materials for catalysis of ORR.

Thioglycolic acid coated on CdTe quantum dots (QDs, emission: 596-604 nm) was exchanged by PVP molecules after incubation of the QDs in PVP solution.²² The PVP-CdTe QDs were assembled into linear chains when dispersed into methanol/acetone/water mixture. CdTe QDs assembled NWs with several to tens of micrometers in length and 30-70 nm in diameters were observed from transmission electron microscopy (TEM) images (Fig. 1a). The high-resolution TEM (HRTEM) image (Fig. S2) displayed discrete lattice fringe that was corresponding to {111} facets of cubic phase CdTe (JCPDS No. 65-1082), revealing that CdTe QDs were randomly assembled into polycrystalline NWs. The assembled structures were not consistent with the previous report, in which occurrence of oriented attachment resulted in the formation of single-crystalline CdTe NWs.²³ Unlike the flexible Au NWs that were bent and encapsulated in a ZIF-8 rhombic dodecahedral nanoparticle,²⁴ the CdTe NWs employed as morphological templates were accountable for ZIF-8 heterogeneous nucleation and growth to form CdTe@ZIF-8 nanofibers. Fig. 1b shows TEM image of the nanofibers with a diameter of 150-200 nm, accompanied with a few isolated ZIF-8 nanoparticles. In contrast to CdTe NWs, the length of CdTe@ZIF-8 nanofibers hardly changed in the encapsulation process. The coarse surfaces revealed that the uniform

^a State Key Laboratory of Fine Chemicals, Dalian University of Technology, Dalian, 116024, PR China. Fax & Tel: 86-411-84986314; E-mail: lychen@dlut.edu.cn; cyduan@dlut.edu.cn.

† Footnotes relating to the title and/or authors should appear here. Electronic Supplementary Information (ESI) available: Experimental details and Fig. S1-9. See DOI: 10.1039/x0xx00000x

nanofiber shells were assembled by a large amount of ZIF-8 polyhedral nanocrystals. Few crevices in dense ZIF-8 shells were found. The amount ratio of ZIF-8 to CdTe played pivotal roles in controlling the assembly structures of composites (Fig. S3). The characteristic diffraction peaks of cubic phase ZIF-8 and cubic phase CdTe were observed from powder X-ray diffraction (PXRD) patterns of nanofibers (Fig. 1c), and no other diffraction peaks of impurity were found.

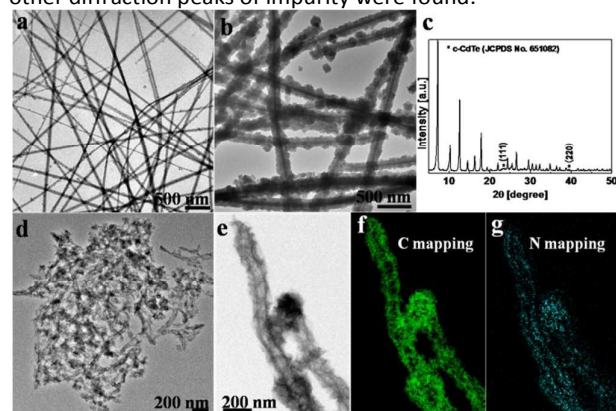


Figure 1. TEM images of (a) CdTe QDs assembled nanowires, (b) CdTe@ZIF-8 nanofibers, and (d, e) One-H/P-C-1000-3 derived from CdTe@ZIF-8 nanofibers; (c) PXRD pattern of CdTe@ZIF-8 nanofibers; (f) C- and (g) N-elemental mappings of (e).

The nanofibers with dense ZIF-8 shells were used to prepare One-H/P-C via heat treatment. From TEM images (Fig. 1d and e), one-dimensional hollow structures with ~ 40 nm of interior diameter were formed and shortened to 1–3 μm in length during pyrolysis of the precursor nanofibers at 1000°C for 3 h (One-H/P-C-1000-3). The formation of hollow structures was attributed to vaporization of CdTe NWs excluded from the composites, and shrinkage of ZIF-8 shells in the carbonization process.^{16, 17} The lattice fringe of about 0.35 nm shown in HRTEM image (Fig. S4) was assigned to the d -spacing of the (002) crystal facet of bulk graphite, indicating that ZIF-8 were transferred into graphitic carbons. The consecutive fringe was not found in the HRTEM image, implying that One-H/P-C-1000-3 was composed of many small graphitic carbons. The graphitic structure was confirmed by PXRD patterns, in which two broad diffraction peaks centered at $\sim 25^\circ$ and $\sim 44^\circ$ were attributed to (002) facet and (110) or (101) facets of graphite, respectively (Fig. S5). To better understand the catalytic activity inducing by anisotropic structures, isolated ZIF-8 nanocrystals with 200–400 nm in diameter were used as precursors to synthesize N-doped graphitic carbons for comparison via pyrolysis (Fig. S6). The skeleton of rhombic dodecahedral ZIF-8 was collapsed at high temperature of 1000°C for 3 h (Z-1000-3), and graphitic carbons characterized by PXRD patterns were formed (Fig. S6).

The crystallinity and graphitization of carbons was greatly dependent on the temperature and duration of carbonization. Albeit salient change of diffraction intensity of (002) facet was hardly observed with increasing pyrolysis temperature, the intensity of (110) or (101) diffraction gradually became stronger, indicating an increase in crystallinity for One-H/P-C

(Fig. S5). Some diffraction peaks located at 26° to 30° and 47° to 56° were present in the PXRD pattern if carbonization was done at 800°C , possibly attributed to residual of templates, confirmed by TEM images (Figure S7). Raman spectrum is an effective tool to characterize graphitic carbons. G band that was assigned to the E_{2g} phonon of graphite was present at $\sim 1585\text{ cm}^{-1}$, and D band for disorder-induced mode of graphite was downshifting to $1320\text{--}1330\text{ cm}^{-1}$ in these samples (Fig. S5).²⁵ The relative intensity change of D band and G band reflected the evolution of graphitic structures (Table S1).²⁶ Similar degree of graphitization for One-H/P-C-1000 with 3 h, 5 h and 10 h based on slight variation of intensity ratio of D to G band for the series (Table S1). Albeit no other impurities were found from these characterizations for One-H/P-C-1000-3, other elements including Zn, Cd, Te and N in final products still needed to be detected by additional characterization techniques. Except for residual Zn element (0.3 wt%), Te and Cd elements were not traced by inductively coupled plasmon atomic emission spectroscopy (ICP-AES). N and C elemental analysis was carried out by energy-dispersive X-ray (EDX) spectroscopy (Fig. 1f and g), exhibiting that N element was uniformly dispersed into one-dimensional carbon domain to form N-doped graphitic carbon materials in element mapping.

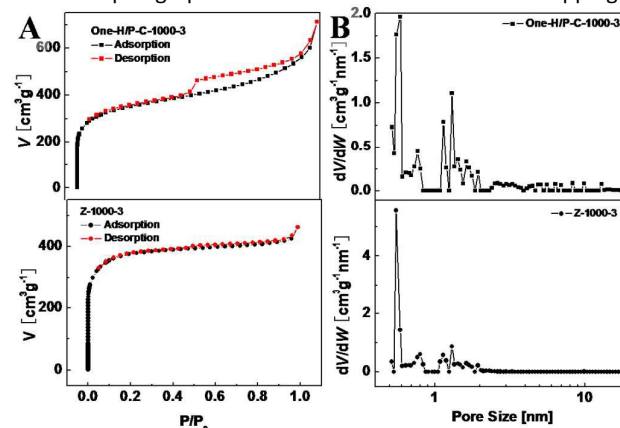


Figure 2. (a) Nitrogen sorption isotherms at 77 K (black, adsorption; red, desorption) and (b) corresponding pore size distribution of One-H/P-C-1000-3 and Z-1000-3.

ORR catalytic activity of graphitic carbons is usually disturbed by their microstructures related to type of pores for mass transport. N_2 sorption isotherm is a powerful technique for characterization of porous structures of solid materials. One-H/P-C-1000-3 and Z-1000-3 exhibited type IV isotherm assigned to mesoporous structures and type I isotherm originated from microporous structures (Fig. 2a), respectively.²⁷ The large hysteresis loop associated with capillary condensation suggested One-H/P-C-1000-3 possesses much high mesopore volume. Nonetheless, the Brunauer-Emmett-Teller (BET) surface area decreased to $1246\text{ m}^2/\text{g}$ for One-H/P-C-1000-3 as compared to Z-1000-3 ($1385\text{ m}^2/\text{g}$). The pore distribution plots (Fig. 2b) showed that well-developed micropores locate in One-H/P-C-1000-3 and Z-1000-3, and the smallest micropores were peaked at 0.6 nm in both samples. Mesopores with different diameters were also able to be

found in One-H/P-C-1000-3 from its pore distribution plot. The microstructures of N-doped graphitic carbons were determined by the assembled structures of precursors, and the mesoporous structures were allowed to be produced from the joint of ZIF-8 nanoparticles on CdTe NWs.²⁸ Transport of O₂, products and electrolyte ions can benefit from these hierarchical porous and hollow structures of One-H/P-C-1000-3 during ORR process, probably accounting for an enhanced electrocatalytic performance.

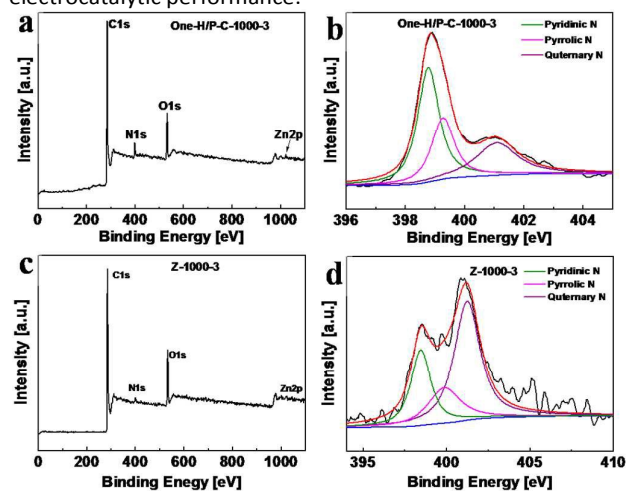


Figure 3. (a, c) XPS survey spectra and (b, d) deconvoluted N1s spectra of One-H/P-C-1000-3 and Z-1000-3, respectively.

Electronic structures of N-doped graphitic carbon can be affected by content and type of N atoms, changing catalytic activity. To confirm the connection type and the content of N atom, X-ray photoelectron spectroscopy (XPS) measurements were performed. The XPS survey spectrum of One-H/P-C-1000-3 (Fig. 3a) displayed not only graphitic C1s, N1s and Zn2p peaks, coinciding with the results of EDX and ICP-AES, but also O1s peaks, which could be attributed to molecules adsorbed on samples such as O₂, H₂O and so on. The atomic ratio of N to C in the sample was about 1/16, far lower than that of precursors from mim (atomic ratio: 1/2). Quaternary N (401.0 eV), pyrrolic N (399.3 eV) and pyridinic N (398.7 eV) were found in the deconvoluted N1s XPS spectrum (Fig. 3b), and the relative amount of Quaternary N was about 26 at%. If N-doped graphitic carbons stemmed from ZIF-8, the similar XPS survey spectrum (Fig. 3c) was obtained. Nevertheless, in contrast to One-H/P-C-1000, the ratio of N to C for Z-1000 was decreased to 1/39. Accordingly, the relative amount of three types of N atoms was also different from that of One-H/P-C-1000-3, and Quaternary N (~53 at%) was the dominant N type in Z-1000-3 (Fig. 3d). Hence, albeit the role of CdTe NWs in preparing N-doped graphitic carbon from ZIF-8 remains elusive, the CdTe@ZIF-8 nanofibers were capable of affecting the type of N atoms and their relative content, as well as the ratio of N to C. We performed cyclic voltammetry (CV) and linear-sweep voltammetry (LSV) measurements in 0.1M KOH aqueous solution to estimate the ORR activity of different carbon-based catalysts as compared to a commercial Pt (20 wt%)/C catalyst

under identical conditions. The CV measurements performed in O₂-saturated KOH solution showed a peak at -0.15 V versus Ag/AgCl for One-H/P-C-1000-3 catalyst, which was about 180 mV more positive than that for Z-1000-3 (Fig. 4a). To gain better insight into the catalytic activity for ORR on different N-doped carbon samples, as well as commercial Pt/C catalyst, LSV tests on a rotating disk electrode (RDE) were carried out (Fig. 4b). The half-wave potential, a benchmark for evaluation of electrocatalytic activity, at the One-H/P-C-1000-3 electrode shown in LSV curve was about -0.17 V, whereas the half-wave potential at Z-1000-3 electrode was negatively shifted to -0.23 V with lower current density at 1600 rpm. These results suggested that One-H/P-C-1000-3 possessed enhanced electrocatalytic activity for ORR. In contrast to Pt/C electrode, One-H/P-C-1000-3 electrode exhibited more negative half-wave potential and higher diffusion-limited current density. Thus, catalytic activity of One-H/P-C-1000-3 was not as good as that of Pt/C towards ORR in terms of half-wave potential, but One-H/P-C-1000-3 stood out as a better ORR catalyst according to diffusion-limited current density. Note that in spite of One-H/P-C-800-3 possessing higher over-potential between -0.2 to -0.3 V as compared with Z-1000-3, it gave a sharp current density increase, leading to its ORR current density exceeding that of Z-1000-3 after -0.3 V.

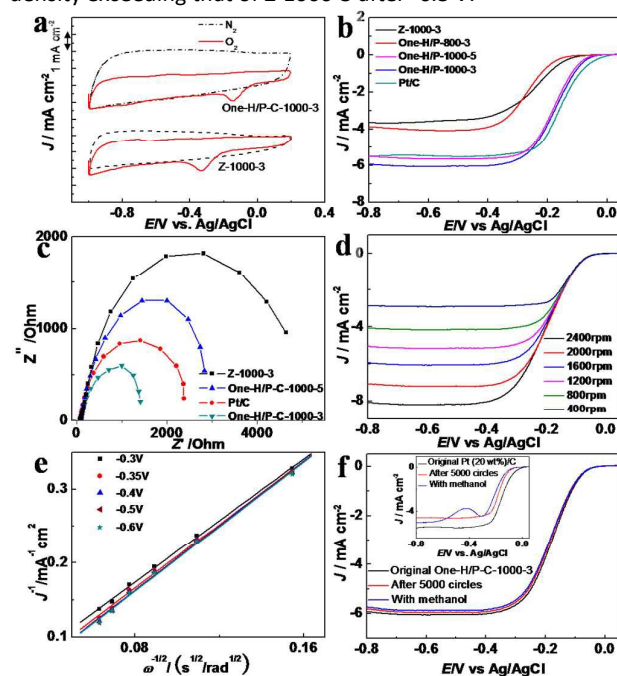


Figure 4. (a) Cyclic voltammograms of One-H/P-C-1000-3 and Z-1000-3, (b) linear sweep voltammograms (LSV) curves of N-doped graphitic carbon series and Pt/C at 1600 rpm, (c) electrochemical impedance spectra measured for One-H/P-C-1000-3 and Z-1000-3, (d) LSV curves of One-H/P-C-1000-3 with different rotation speeds, (e) K-L plots of One-H/P-C-1000-3 at different potentials, and (f) stability experiments of One-H/P-C-1000-3 via 5000 circles and adding methanol after circling. Inset of (f) is stability experiments of Pt/C via 5000 cycles and adding methanol after cycling. All measurements were carried out using a glassy carbon electrode at a catalyst loading of ~0.15 mg/cm² in O₂ saturated 0.1 M KOH aqueous solution at a scan rate of 10 mV s⁻¹.

Pyrolysis temperature and duration inducing different microstructures of N-doped carbons obtained were key factors in affecting the electrocatalytic activity for ORR. The diffusion-limited current density and half-wave potential increased with increasing pyrolysis temperature shown in LSV plots at 1600 rpm (Fig. 4b). Hence, One-H/P-C-1000-3 as ORR catalyst is superior to other catalysts among series. The similar half-wave potential and different diffusion-limited current density between One-H/P-C-1000-3 and -5 electrodes could be caused by damage of one-dimensional graphitic carbon structures with longer heat treatment time (Fig. S8). Therefore, carbonization of CdTe@ZIF-8 at 1000 °C for 3 h is optimal conditions to construct N-doped graphitic carbons with high electrocatalytic activity for ORR, which could be attributed to the balance of degree of graphitization, density of active sites and completeness of structures. Given anisotropic structures enabling to help N-doped graphitic carbons better contact and prevent their aggregation during ORR process, One-H/P-C-1000-3 electrode possessed much lower intrinsic resistance than that of other electrodes.

In comparison with other electrocatalysts in our case, One-H/P-C-1000-3 exhibit high limiting current density. Occurrence of the phenomena could depend on the electron-transfer resistance, which was characterized by the electrochemical impedance spectroscopy (EIS) (Fig. 4c). These semicircles of Nyquist plots at the tested frequency range corresponded to the electron-transfer resistance. The resistance was derived from the diameters of semicircles of EIS. Hence, One-H/P-C-1000-3 possessed the smallest electron-transfer resistance based on the semicircle with the smallest diameter.

Figure 4d showed the LSV curves at different rotation rates for One-H/P-C-1000-3 electrode, and diffusion-limited current density increased with increase of rotation rates. To provide an insight into the superior electrochemical performance of One-H/P-C-1000-3, the reaction kinetics and the number of electron transfer for every oxygen molecule needed to be examined according to the corresponding Koutecky-Levich (K-L) plots within the potential range from -0.3 V to -0.6 V in these LSV curves. All K-L plots exhibited good linearity with similar slopes (Fig. 4e). Thus One-H/P-C-1000-3 as electrocatalysts for ORR was corresponding to first-order reaction kinetics with regard to O₂ concentration in KOH aqueous solution. The electron transfer number was up to 3.96 obtained at as low as -0.35 V, and the value bore comparison with that of Pt/C (3.97, Fig. S9) at -0.35 V. The average value reached to 3.90 at low over-potential ranging from -0.3 V to -0.6 V, suggesting that O₂ was reduced via a dominant one-step four-electron pathway. In contrast to One-H/P-C-1000-3, Z-1000-3 exhibited lower value for the number of electron transfer (2.82 at -0.35 V), suggesting that the dominant ORR process involved in a two-electron pathway.

To assess the electrocatalytic durability, One-H/P-C-1000-3 electrode was cycled between 0.2 V and -1.0 V in O₂ saturated 0.1 M KOH solution at a scan rate of 50 mV s⁻¹. After 5000 consecutive-cycle operation, slight fluctuation of voltammetric current and potential were found in One-H/P-C-1000-3 electrode. The half-wave potential was negatively shift to

around 5 mV, and the diffusion-limited current still retained up to 98% as compared to original values of One-H/P-C-1000-3 (Fig. 4f). In comparison with the Pt/C electrocatalyst, the strong change of current density and potential took place after 5000 cycles (inset of Fig. 4f). The enhanced durability of One-H/P-C-1000-3 could be attributed to its stable structures minimizing the leaching/aggregation of active sites. Applications of Pt/C in ORR-related energy storage and conversion devices were severely restricted by methanol crossover (inset of Fig. 4f).²⁹ If injecting 3 mL of 3 M methanol into electrolyte solution after One-H/P-C-1000-3 electrode performed 5000 cycles, little change of diffusion-limited current density and half-wave potential of ORR occurred (Fig. 4f). These results reveal that One-H/P-C-1000-3 has high stability for ORR, for long-time continuous catalysis, as well as strong tolerance to methanol crossover. On this basis, One-H/P-C-1000-3 can be potentially used as cathode catalysts for direct methanol fuel cells.

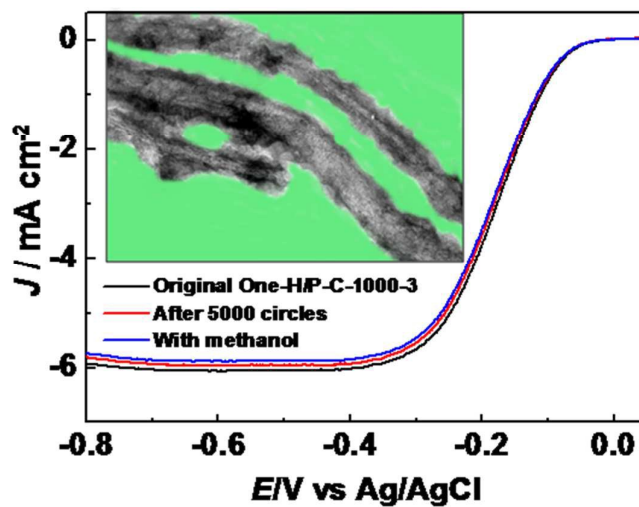
In conclusion, electrocatalyst's performance towards ORR is usually affected by three aspects: thermodynamic aspect of free energy for elementary reaction steps of O₂ reduction into H₂O; kinetic aspect of the rate of O₂ diffusion and adsorption and electron transport; stability and density of catalytic sites. In our study, a synthetic strategy to One-H/P-C by pyrolysis of CdTe@ZIF-8 nanofibers was developed. One-H/P-C-1000-3 exhibited more positive half-wave potential and higher limiting current density as compared to Z-1000-3. The superior electrocatalytic performance could be originated from high content of N element generating high density of catalytic sites, one-dimensional structures inducing continuous electron transport, and hierarchical porous and hollow structures facilitating transport of electrolyte, products and O₂. In spite of catalytic activity on One-H/P-C-1000-3 slightly inferior to Pt(20 wt%)/C in term of half-wave potential, the unique morphology and the stable structures can minimize electron-transfer resistance and leaching/aggregation of active sites, leading to high diffusion-limited current density and high stability after numerous cycles or introducing methanol.

We acknowledge financial support from the Research Groups of the National Natural Science Foundation of China (21421005), the Specialized Research Fund for the Doctoral Program of Higher Education of China (20130041120025), the Fundamental Research Funds for the Central Universities (DUT15LK04), and the Foundation of the Ministry of Education of China for Returned Scholars.

Notes and references

- 1 J. Masa, W. Xia, M. Muhler and W. Schuhmann, *Angew. Chem. Int. Ed.*, 2015, **54**, 10102-10120.
- 2 W. Ai, Z. Luo, J. Jiang, J. Zhu, Z. Du, Z. Fan, L. Xie, H. Zhang, W. Huang and T. Yu, *Adv. Mater.*, 2014, **26**, 6186-+.
- 3 Y. J. Sa, C. Park, H. Y. Jeong, S.-H. Park, Z. Lee, K. T. Kim, G.-G. Park and S. H. Joo, *Angew. Chem. Int. Ed.*, 2014, **53**, 4102-4106.
- 4 M. K. Debe, *Nature*, 2012, **486**, 43-51.

- 5 B. Lim, M. Jiang, P. H. C. Camargo, E. C. Cho, J. Tao, X. Lu, Y. Zhu and Y. Xia, *Science*, 2009, **324**, 1302-1305.
- 6 L. Zhang, R. Iyyamperumal, D. F. Yancey, R. M. Crooks and G. Henkelman, *ACS Nano*, 2013, **7**, 9168-9172.
- 7 Y. Zheng, Y. Jiao, M. Jaroniec, Y. Jin and S. Z. Qiao, *Small*, 2012, **8**, 3550-3566.
- 8 X. Zhou, J. Qiao, L. Yang and J. Zhang, *Adv. Energy Mater.*, 2014, **4**.
- 9 L. Dai, Y. Xue, L. Qu, H.-J. Choi and J.-B. Baek, *Chem. Rev.*, 2015, **115**, 4823-4892.
- 10 H.-W. Liang, X. Zhuang, S. Bruller, X. Feng and K. Mullen, *Nat. Commun.*, 2014, **5**, 4973-4973.
- 11 H.-W. Liang, W. Wei, Z.-S. Wu, X. Feng and K. Muellen, *J. Am. Chem. Soc.*, 2013, **135**, 16002-16005.
- 12 L. Zhang, Z. Su, F. Jiang, L. Yang, J. Qian, Y. Zhou, W. Li and M. Hong, *Nanoscale*, 2014, **6**, 6590-6602.
- 13 S. Wang, L. Zhang, Z. Xia, A. Roy, D. W. Chang, J.-B. Baek and L. Dai, *Angew. Chem. Int. Ed.*, 2012, **51**, 4209-4212.
- 14 Z.-S. Wu, W. Ren, L. Xu, F. Li and H.-M. Cheng, *ACS Nano*, 2011, **5**, 5463-5471.
- 15 W. Yang, X. Liu, X. Yue, J. Jia and S. Guo, *J. Am. Chem. Soc.*, 2015, **137**, 1436-1439.
- 16 W. Zhang, Z.-Y. Wu, H.-L. Jiang and S.-H. Yu, *J. Am. Chem. Soc.*, 2014, **136**, 14385-14388.
- 17 B. Liu, H. Shioyama, T. Akita and Q. Xu, *J. Am. Chem. Soc.*, 2008, **130**, 5390-+.
- 18 W. Chaikittisilp, M. Hu, H. Wang, H.-S. Huang, T. Fujita, K. C. W. Wu, L.-C. Chen, Y. Yamauchi and K. Ariga, *Chem. Commun.*, 2012, **48**, 7259-7261.
- 19 H.-x. Zhong, J. Wang, Y.-w. Zhang, W.-l. Xu, W. Xing, D. Xu, Y.-f. Zhang and X.-b. Zhang, *Angew. Chem. Int. Ed.*, 2014, **53**, 14235-14239.
- 20 K. S. Park, Z. Ni, A. P. Cote, J. Y. Choi, R. Huang, F. J. Uribe-Romo, H. K. Chae, M. O'Keeffe and O. M. Yaghi, *Proc. Natl. Acad. Sci. U.S.A.*, 2006, **103**, 10186-10191.
- 21 Y. Wang, J. He, C. Liu, W. H. Chong and H. Chen, *Angew. Chem. Int. Ed.*, 2015, **54**, 2022-2051.
- 22 G. Lu, S. Li, Z. Guo, O. K. Farha, B. G. Hauser, X. Qi, Y. Wang, X. Wang, S. Han, X. Liu, J. S. DuChene, H. Zhang, Q. Zhang, X. Chen, J. Ma, S. C. J. Loo, W. D. Wei, Y. Yang, J. T. Hupp and F. Huo, *Nat. Chem.*, 2012, **4**, 310-316.
- 23 Z. Y. Tang, N. A. Kotov and M. Giersig, *Science*, 2002, **297**, 237-240.
- 24 W. Zhang, Y. Liu, G. Lu, Y. Wang, S. Li, C. Cui, J. Wu, Z. Xu, D. Tian, W. Huang, J. S. DuCheneu, W. D. Wei, H. Chen, Y. Yang and F. Huo, *Adv. Mater.*, 2015, **27**, 2923-+.
- 25 H. Abramczyk and B. Brozek-Pluska, *Chem. Rev.*, 2013, **113**, 5766-5781.
- 26 A. C. Ferrari, J. C. Meyer, V. Scardaci, C. Casiraghi, M. Lazzeri, F. Mauri, S. Piscanec, D. Jiang, K. S. Novoselov, S. Roth and A. K. Geim, *Phys. Rev. Lett.*, 2006, **97**.
- 27 N. C. Burtch, H. Jasuja and K. S. Walton, *Chem. Rev.*, 2014, **114**, 10575-10612.
- 28 H.-L. Jiang, B. Liu, Y.-Q. Lan, K. Kuratani, T. Akita, H. Shioyama, F. Zong and Q. Xu, *J. Am. Chem. Soc.*, 2011, **133**, 11854-11857.
- 29 Y. Bing, H. Liu, L. Zhang, D. Ghosh and J. Zhang, *Chem. Soc. Rev.*, 2010, **39**, 2184-2202.



Hierarchical porous and hollow N-doped graphitic carbons with one-dimensional structures were successfully achieved by a sacrificial template method. The materials exhibited an enhanced electrocatalytic performance towards ORR due to one-dimensional structures inducing continuous electron transport, and hierarchical porous and hollow structures facilitating transport of electrolyte, products and O₂.